Applied Catalysis B: Environmental 218 (2017) 452–459

Contents lists available at ScienceDirect

Applied Catalysis B: Environmental

journal homepage: www.elsevier.com/locate/apcatb

Synthesis of CdS-decorated MIL-68(Fe) nanocomposites: Efficient and stable visible light photocatalysts for the selective reduction of 4-nitroaniline to *p*-phenylenediamine in water

Ruowen Liang[a,b], Fenfen Jing[a], Guiyang Yan[b], Ling Wu[a,*]

[a] State Key Laboratory of Photocatalysis on Energy and Environment, Fuzhou University, Fuzhou 350002, PR China
[b] Department of Chemistry, Fujian Province University Key Laboratory of Green Energy and Environment Catalysis, Ningde Normal University, Ningde 352100, PR China

ARTICLE INFO

Article history:
Received 26 April 2017
Received in revised form 21 June 2017
Accepted 24 June 2017
Available online 27 June 2017

Keywords:
MIL-68(Fe)
CdS
4-Nitroaniline
Visible light
Selective reduction

ABSTRACT

Visible-light-initiated organic transformations have received much attention because of low cost, relative safety, and environmental friendliness. In this work, a series of CdS-decorated MIL-68(Fe) nanocomposites (CdS-M68 NCs) have been prepared via a facile room-temperature photodeposition technique in a controlled manner. Importantly, the CdS-M68 NCs exhibit remarkably enhanced photoactivity toward selective reduction of 4-nitroaniline (4-NA) to *p*-phenylenediamine (PPD) in water under visible light irradiation ($\lambda \geq 420$ nm) as compared to bare CdS and MIL-68(Fe), giving a 4-NA conversion of ~100% after irradiation for 8 min. The significantly enhanced photoactivity is attributed to the integrated factors of the effective transportation of the photogenerated electron-hole pairs and the enhanced visible light absorption intensity. Combining with trapping experiments and ESR analysis, it could be revealed that the photoexcited electrons and $^{\bullet}CO^{2-}$ radicals should be the main active species in the present system. In addition, a possible photocatalytic reduction mechanism has been investigated.

1. Introduction

Aminobenzenes are an important class of industrial intermediates for a variety of industrial chemicals. *p*-phenylenediamine (PPD), as a member of the aminobenzenes, is a useful ingredient to many industrial chemicals (*e.g.,* rubber antioxidants, textile fibers and thermoplastics) [1–3]. In the past, direct catalytic hydrogenation of 4-nitroaniline (4-NA) has been proved to be an effective process for the preparation of PPD [1]. However, this process suffers from the limitations of rigorous reaction conditions, high costs and tedious procedures. Therefore, developing general, economic and simple routes for the preparation of PPD is required. Recently, various methods, such as electrochemical systems and photocatalysis, have been reported for the preparation of aminobenzenes [4–6]. Among these methods, visible-light photocatalysis has emerged as a powerful technique since it achieves the one-pot preparation of aminobenzenes by reducing nitrobenzenes in water under sunlight irradiation.

Up to now, numerous photocatalysts have been discovered for this reaction. Cadmium sulfide (CdS) is one of the most promising materials, which has been studied widely due to its visible light response and appropriate position of conduction band. Nevertheless, the fast recombination of photogenerated electron-hole pairs and the lack of catalytic sites are two key factors that hinder the enhancement of photocatalytic performance of pure CdS [7]. Many attempts have been made to enhance the activity of CdS, such as nanostructuring and coupling with other materials. Actually, combining CdS with other semiconductors to construct heterostructures (*e.g.* CdS-SnO_2, CdS-TiO_2, CdS-C_3N_4) is considered as one of the best approaches to suppress the recombination of photogenerated charge carriers [8–11]. However, the common CdS-semiconductor hybrids often suffered from the drawbacks of poor interface contact, low specific surface area, lack of catalytic sites and reaction centers. Thus, there is still plenty of room to explore unfulfilled potentials for improving the fabrication and properties of CdS-based photocatalysts.

Metal-organic frameworks (MOFs) are a class of crystalline materials formed by transition metal-containing clusters as structural nodes bridged by organic linkers. [12]. As the historic work made by García et al. on UV light induced phenol photodegradation using MOF-5 as a semiconductor in 2006, a range of photoactive

* Corresponding author.
E-mail address: wuling@fzu.edu.cn (L. Wu).

http://dx.doi.org/10.1016/j.apcatb.2017.06.075
0926-3373/

MOFs have been discussed by researchers with great enthusiasm [13–17]. In our previous study, we have also shown that the MIL-68(Fe) could serve as a type of efficient photocatalysts for photocatalytic reduction reaction driven by visible light irradiation [18]. Compared with traditional semiconductor photocatalysts, the superiority of the photosensitive MOFs as supporters for CdS lie in the fact that (i) ultrahigh surface area can be expected on such hybrid materials; (ii) the narrow micropore distribution may lead to the formation of monodisperse CdS particles. More importantly, it could be expected that a photoactive MOF can not only serve as a host to control the encapsulation of CdS, but also facilitate the separation of photogenerated charge carriers by forming the effective interfacial contact with CdS when the two components have well-matched band structures [19,20]. Although there have been some reports on semiconductor-MOFs naocomposites (NCs) [21–23], it should be noted that the reports on CdS-MOFs NCs for photocatalytic applications are rather scarce. Especially, the unique CdS-MOFs NCs into photocatalytic selective reduction of nitro organics under visible light, to the best of our knowledge, have not been thoroughly investigated.

Herein, we report for the first time the synthesis of CdS-decorated MIL-68(Fe) *via* a facile photodeposition method. MIL-68(Fe), which consists of chains of cornersharing Fe-O octahedra connected through 1,4-benzenedicarboxylic acid linker, possesses with high stability [18,24]. Moreover, its photocatalytic makes it as an intriguing candidate for our study. The as-synthesized CdS-MIL-68(Fe) (denoted as CdS-M68) NCs have exhibited remarkably enhanced visible light photoactivities toward selective reduction of nitro organic as compared to the original MIL-68(Fe) and CdS. The origin accounting for the improved photoactivity and the underlying reaction mechanism have been studied in terms of a series of characterizations and controlled experiments using radical scavengers. Finally, a possible reaction mechanism of photocatalytic reduction of 4-NA to PPD in solutions through CdS-M68 NCs have also been investigated in detail. It is expected that our current research could provide a new way to design MOF-semiconductor photocatalysts and their applications as visible light photocatalysts toward selective organic transformations.

2. Experimental

2.1. Materials and reagents

Iron(III) chloride hexahydrate ($FeCl_3{\cdot}6H_2O$) was supplied by Aladdin Reagent Co., Ltd. 1,4-benzenedicarboxylic acid (H_2BDC) was obtained from Alfa Aesar China Co., Ltd., cadmium chloride ($CdCl_2{\cdot}5H_2O$), elemental sulfur (S_8), hydrofluoric acid (HF, 49%), hydrochloric acid (HCl), N,N-Dimethylformamide (DMF), acetone, ethanol and ammonium formate (HCO_2NH_4) were obtained from Sinopharm Chemical Reagent Co., Ltd. (Shanghai, China). All materials were used as received without further purification.

2.2. Synthesis of MIL-68(Fe) samples

MIL-68(Fe) was obtained according to the strategy that reported in previous [18]. A mount of $FeCl_3{\cdot}6H_2O$ and H_2BDC (molar ratio = 1:2) were mixed with 12 mL DMF in a Teflon-lined autoclave, then 120 μL HF (5 mmol) and 120 μL HCl (1 mmol) were added, followed stirring for another 30 min to blend completely. After that, the Teflon-lined was heated at 100 °C for 120 h. The products were left cool at room temperature, collected by centrifugation and washed with deionized water and acetone several times to eliminate the DMF molecules in the pores. Finally, the recovered solid was dried at 100 °C vacuum oven for 24 h.

2.3. Fabrication of CdS-MIL-68(Fe) NCs

The CdS-MIL-68(Fe) NCs were synthesized by a photodeposition method. First, a certain amount of the MIL-68(Fe) was evenly dispersed in 25 mL of absolute ethanol. Then, we added 10 mg of S_8 and 78 mg of $CdCl_2{\cdot}5H_2O$ and bubbled with nitrogen for 30 min in the dark. Last, the suspension was irradiated with a 300 W Xe arc lamp with incident light at $\lambda \geq 420$ nm for 2, 4, or 6 h. The obtained samples were labeled as X-CdS-M68, where X = 2, 4 and 6 according the photodeposition time.

2.4. Characterizations

The X-ray diffraction (XRD) patterns of the samples were carried on a Bruker D8 Advance X-ray diffrractometer operated at 40 kV and 40 mA with Ni-filtered Cu Ka irradiation. The data were recorded in the 2θ ranging from 3° to 70° with a step width of 0.05°. The Brunauer-Emmett-Teller (BET) surface area was measured with an ASAP2020 M apparatus (Micromeritics Instrument Corp., USA). Before the test, the samples were degassed in vacuum at 120 °C for 6 h. The nitrogen adsorption and desorption isotherms were measured at 77 K. UV–vis diffuse reflectance spectra (UV-vis DRS) were obtained by a Cary 500 UV-vis-NIR spectrophotometer in which $BaSO_4$ powder was used as the internal standard to obtain the optical properties of the samples over a wavelength range of 330–650 nm. X-ray photoelectron spectroscopy (XPS) measurements were conducted on a PHI Quantum 2000 XPS system equipped with a monochromatic Al Kα X-ray source to obtain the surface elemental composition of the sample. The Mott-Schottky analysis was performed at a Zenuium electrochemical workstation. The electrochemical measurements were performed in a conventional three electrode cell, Ag/AgCl electrode was used as the reference electrode and a Pt plate was used as the counter electrode. The photocurrent measurements were conducted with a BAS Epsilon workstation. The Mott-Schottky experiments were conducted on a Precision PARC workstation. Electron spin resonance (ESR) signals of spin-trapped paramagnetic species with 5,5-dimethyl-1-pyrrolineN-oxide (DMPO) were recorded with a Brucker A300 spectrometer. A 300 W Xe lamp (Beijing Perfectlight, PLS-SXE300c) with a 420 nm cut-off filter was used as a light source.

2.5. Evaluation of photocatalytic activity

For the photocatalytic reduction of 4-nitroaniline (4-NA) and *p*-phenylenediamine (PPD), an ozone-free 300 W Xe lamp (PLS-SXE300C, Trusttech Co. Ltd, Beijing) with a cut off filter of 420 nm and an infrared filter was used as the light source ($\lambda \geq 420$ nm). Prior to the catalytic test, 40 mg of photocatalyst was suspended in 40 mL of 4-NA (A.R., Alfa Aesar Co.) aqueous solution (20 mg/L) in a glass reactor (100 mL). Nitrogen was then purged through the system, followed by the introduction of 20 mg of HCO_2NH_4. After that, the suspension was stirred in the dark for 1 h to ensure the establishment of adsorption-desorption equilibrium between the sample and 4-NA. As the reaction proceeded, 3 mL of the suspension was taken at a certain interval and was centrifuged (12000 rpm, 2 min). The 4-NA and PPD concentrations during the reaction were analyzed by measuring the absorbance at 380 and 238 nm with a Cary 50 UV–vis spectrophotometer (Varian Co.), respectively. The reactant and product identification were also confirmed by the high performance liquid chromatography (HPLC, Agilent 1260). Separation was carried out at about 23 °C on the Xtimate™ C18 column (4.6 mm × 150 mm, 5.0 μm particle size). The mobile phase consisted of H_2O-acetonitrile solution (75:25, v/v), at a flow rate of 0.8 mL/min, the wavelength for detection was adjusted to 228 nm.

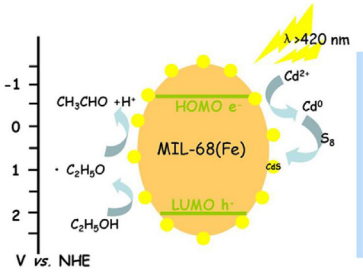

$$MIL\text{-}68(Fe) + h\nu \rightarrow MIL\text{-}68(Fe)\,(h^+ + e^-) \quad \text{Eq. (1)}$$

$$h^+ + C_2H_5OH \rightarrow \bullet C_2H_5O + H^+ \quad \text{Eq. (2)}$$

$$\bullet C_2H_5O + h^+ \rightarrow CH_3CHO + H^+ \quad \text{Eq. (3)}$$

$$Cd^{2+} + 2\,e^- \rightarrow Cd^0 \quad \text{Eq. (4)}$$

$$Cd^0 + S_x \rightarrow CdS + S_{x-1}\,(x \leq 8) \quad \text{Eq. (5)}$$

Scheme 1. Overall flowchart for fabrication of the CdS-M68 NCs *via* a facile photodeposition approach.

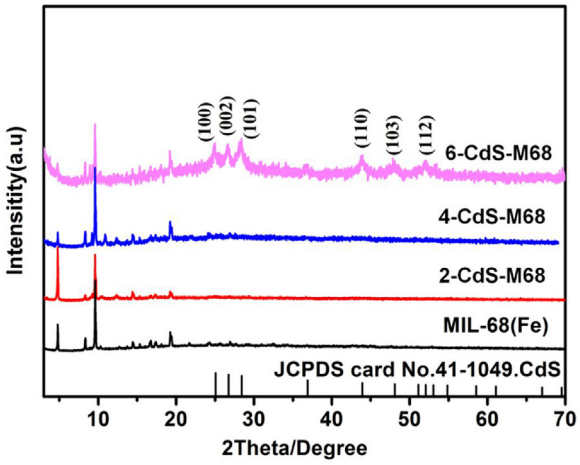

Fig. 1. XRD patterns of MIL-68(Fe) and the CdS-M68 NCs prepared with different photodeposition times under visible light ($\lambda \geq 420$ nm).

3. Results and discussion

3.1. Characterizations

CdS particles deposited on MIL-68(Fe), denoted as CdS-M68, have been prepared *via* a facile room-temperature photodeposition method, as illustrated in Scheme 1. Once MIL-68(Fe) is dispersed in absolute ethanol and subsequently irradiated by visible light ($\lambda \geq 420$ nm), the photogenerated holes are scavenged by ethanol while the photogenerated electrons are trapped by Cd^{2+} ions to form Cd^0. Then the Cd^0 reacts with S_x to obtain CdS. Meanwhile, CdS-M68 NCs with intimate interfacial contact are obtained.

Fig. 1 shows the XRD patterns of pure CdS and CdS-M68 NCs. The diffraction peaks of MIL-68(Fe) match well with the calculated ones, indicating that the obtained samples are pure phase [18]. As for the CdS-M68 NCs, it is clear to see that the introduction of MIL-68(Fe) almost has no effect on the crystallinity of the samples, which is logical for the following reasons: (i) the percentage of CdS accounted for the CdS-M68 NCs is relatively small; (ii) the in situ process should lead to a uniform distribution of CdS particles, which can explain the absence of CdS diffraction peaks for the samples with small amount of CdS; (iii) the treatment temperature for forming CdS phase is lower than that of preparing MIL-68(Fe). When the photodeposition time of CdS is increased up to 6 h, the main peak of hawleyite CdS phase (JCPDS No. 10-0454) at 24.8°, 26.5°, 28.2°, 43.9°, 48.2 and 52.1° can be observed. For the CdS-M68 NCs samples, it can also be found that the intensity of the diffraction peaks are decreased with increasing in the photodeposition time, which might be due to the occupation of CdS on the surface of MIL-68(Fe).

To verify further the microscopic structure of the CdS-M68 NCs, TEM images have been taken. As shown in Fig. 2(a), the MIL-68(Fe) substrate displays some sheets nanocrystals. Fig. 2(b)-(d) show typical TEM images of the samples obtained with different photodeposition times from 2 to 6 h, respectively. It is apparent that MIL-68(Fe) serves as support and no significant change of the characteristic structure of MIL-68(Fe) is observed after CdS loading. It clearly shows that with the photodeposition time prolonged 2–4 h, more CdS particles are found to decorate the surface of MIL-68(Fe). A high dispersion of CdS with the particle sizes of range from 4 to 8 nm can be observed (see Fig. S1). Moreover, the interfacial contact between MIL-68(Fe) and CdS is intimate. Notably, when the irradiation time is increased to 6 h, the CdS particles aggregate to a large degree. High-resolution TEM (HRTEM) images of 4-CdS-M68 are shown in Fig. 2(e) and (f). The lattice spacing of d = 0.336 nm and d = 0.368 nm matches that of the (0 0 2) and (1 0 0) crystallographic plane of hexagonal CdS, respectively. Furthermore, the amount of CdS deposited on MIL-68(Fe) has been determined by ICP. It is found that the loading percentage of CdS in samples of 2-CdS-M68, 4-CdS-M68 and 6-CdS-M68 are 4.88%, 16.03%, 22.60%, respectively.

Table 1
The CdS loading ratio, BET surface area and pore volume of CdS-M68 NCs with different photodeposition time.

Samples	CdS(wt%)	S_{BET} (m^2/g)	Pore volume (cm^3/g)
MIL-68	0	206.58	0.197
2-CdS-M68.	4.88	142.82	0.117
4- CdS-M68	16.03	69.56	0.079
6-CdS-M68	22.60	45.52	0.085

Surface chemical compositions of a typical sample (sample 4-CdS-M68) have been studied by XPS. As shown in Fig. 3(a), the survey spectrum of the 4-CdS-M68 shows the pronounced featured signal of Cd 3d, S 2p, Fe 2p, O 1s, and C 1s, indicating that the CdS particles are successfully immobilized on the surface of the MIL-68(Fe). The binding energies of 405.4 and 412.1 eV for Cd $3d_{5/2}$ and Cd $3d_{3/2}$ confirm a bivalent oxidation state for Cd (see Fig. 3(b)). It is also found that the binding energy of S 2p is 161.5 eV, indicating that a S^{2-} oxidation state exists on the sample surface (see Fig. 3(c)). Fig. 3(d) shows the high-resolution XPS spectra of Fe 2p. The binding energies of 712.1 and 726.0 eV with a satellite signal at 719.0 eV are characteristic of Fe(III) in MIL-100(Fe). The peak separation, namely, $\Delta = 2p_{1/2} - 2p_{3/2} = 13.9$ eV, which is very similar to those reported for α-Fe_2O_3 [25]. Therefore, the joint results of XRD, TEM, ICP and XPS verify the CdS-M68 NCs have been successfully prepared *via* the photodeposition approach. Moreover, the current approach for introducing the second component is effective, which can preserve the structural property of the basic composite.

In addition, the specific Brunauer-Emmett-Teller (BET) surface area and pore structure of the prepared samples have been investigated (see Fig. S2 and Table 1). The BET surface area of MIL-68(Fe) is 206.58 m^2/g. the BET surface area of the samples gradually decreases with increasing CdS content, from 206.58 to 45.52 m^2/g. Although the BET surface area of CdS-M68 is smaller than that of MIL-68(Fe), it is still much higher than other CdS and CdS-based materials. It is expected that a greater specific surface area of photocatalysts can supply more surface active sites and make charge

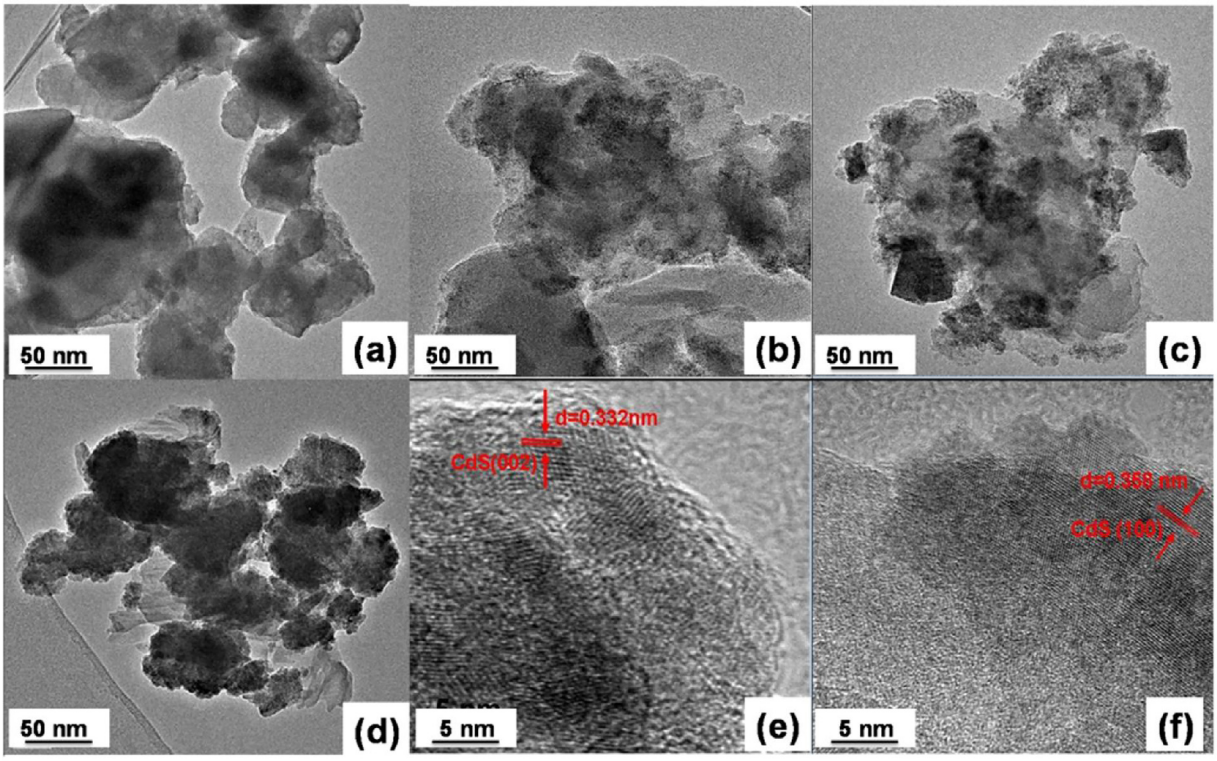

Fig. 2. TEM images of (a) MIL-68(Fe), (b, c, d) X-CdS-M68 NCs (X = 2, 4, 6) and (e, f) HRTEM images of the as-prepared 4-CdS-M68 NCs.

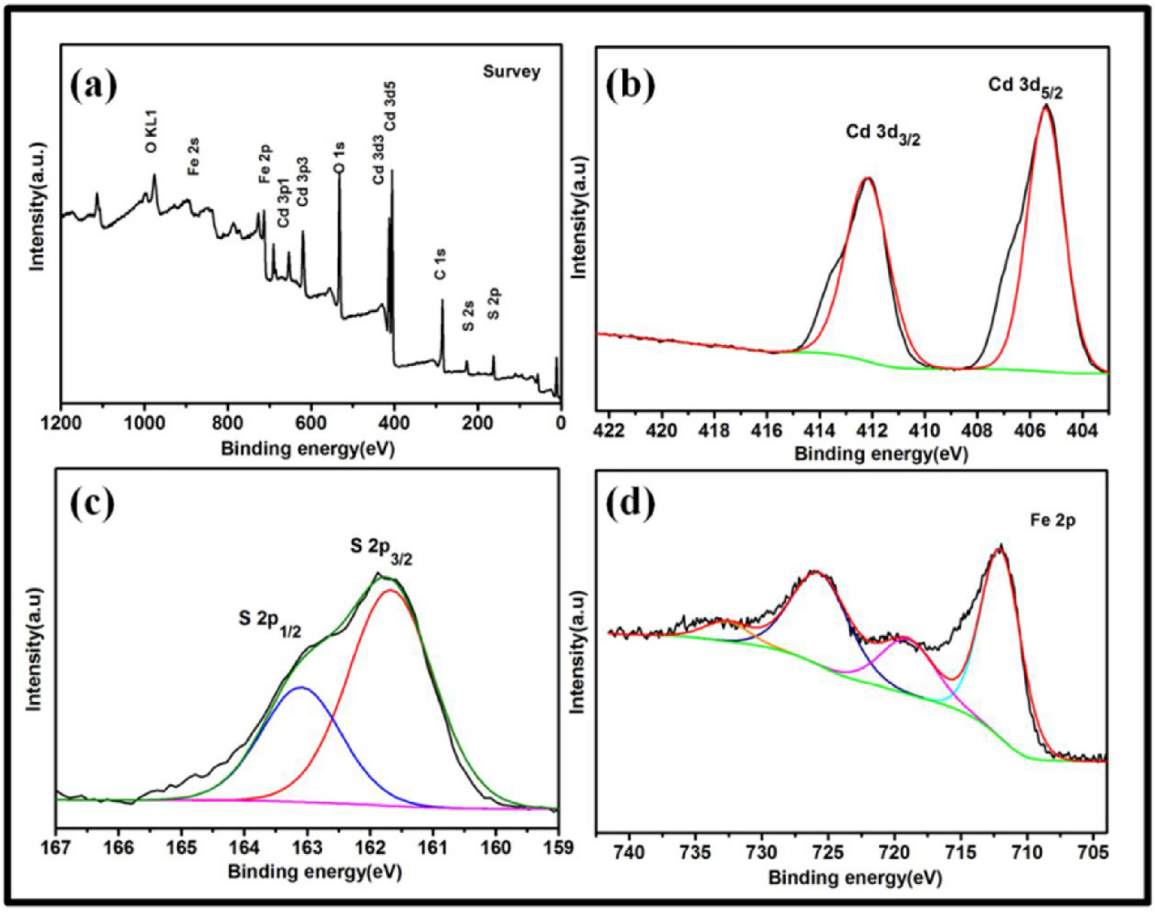

Fig. 3. XPS patterns of 4-CdS-M68.

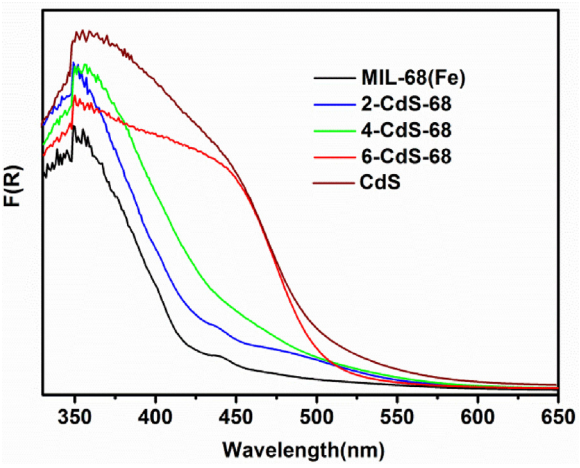

Fig. 4. UV–vis absorption spectra of MIL-68(Fe), CdS and CdS-M68 NCs.

carrier transport easier, leading to an enhancement of the photocatalytic performance. The optical properties of CdS-M68 NCs have been measured using ultraviolet-visible light diffuse reflectance spectra (UV-vis DRS). As display in Fig. 4, the absorption-band positions of MIL-100(Fe) in the UV region are ascribed to π-π* transitions of ligands, whereas the absorption band in the visible region belongs to the ligand to metal charge transfer transitions (LMCT) from H_2BDC ligands to Fe^{3+} centers [26–28]. After introduction of CdS, the absorption of the samples in the visible light region can be enhanced by increasing the photodeposition time. This can be attributed to the increase in the amount of CdS in the as-prepared samples, because CdS is a well-known visible-light-induced photocatalyst (band gap ~2.4 eV) [29]. Therefore, the enhanced absorbance of light is expected to improve the visible-light-driven photocatalytic activity for a target reaction.

3.2. Photocatalytic properties

The photocatalytic performance of CdS-M68 NCs has been evaluated toward selective reduction of nitro organic 4-NA to its corresponding amino organic PPD in the aqueous phase under visible light irradiation (λ ≥ 420 nm) using HCO_2NH_4 as quencher for photogenerated holes and N_2 purge under ambient conditions. Fig. S3(a) shows the temporal evolution of the spectral changes during the photocatalytic reduction of 4-NA over CdS-M68 photocatalysts under visible light (λ ≥ 420 nm). There is a rapid decrease in the absorption of 4-NA at 380 nm, indicating that 4-NA can be reduced by the 4-CdS-M68. This is further corroborated by the high-performance liquid chromatographic (HPLC) analysis (see Fig. S3(b)). It can be seen that the product is primarily dominated by 4-PDA, giving a high PPD selectivity.

Control experiments have been first carried out to demonstrate the photocatalytic nature of the reactions. As shown in Fig. 5(a), in the absence of catalyst or light lead to no conversion of substrate 4-NA, which ensures that the reaction is driven by a photocatalytic process. As a part of this work, the effects of the addition of HCO_2NH_4 and the N_2 atmosphere on the photoreduction of 4-NA over 4-CdS-M68 photocatalyst were investigated. As displayed in Fig. 5(b), no significant reaction of 4-NA is observed after 8 min of visible light irradiation neither in the presence of 4-CdS-M68 and HCO_2NH_4 (23.1%), or in the presence of 4-CdS-M68 photocatalyst upon purging with N_2 (29.5%). However, 4-NA is rapidly reduced to PPD in the presence of 4-CdS-M68 and HCO_2NH_4 upon purging with N_2 under visible light irradiation (~100%). Evidently, both the addition of HCO_2NH_4 and the N_2 atmosphere are indispensable for the photocatalytic reduction of 4-NA over the 4-CdS-M68 photocatalyst in this work.

Fig. 6(a) shows the photocatalytic activities of CdS-M68 NCs with photodeposition time changing from 2 to 6 h. Taking a view of the overall activities, it can be seen that when the photodeposition time is prolonged to 4 h, the optimal photocatalytic performance is obtained, the reduction efficiency is rapidly increased to 99.5% after visible light illumination for 8 min. It is also higher than that of higher than that of MIL-68(Fe), CdS and CdS + MIL-68(Fe) (prepared by simply mixing MIL-68(Fe) and CdS in proper proportions under identical conditions). To quantitatively understand the reaction kinetics of the photocatalytic reduction of 4-NA to 4-PDA in our experiments, we applied the pseudo-first order model: $\ln(C_0/C_t) = kt$, which is generally used for photocatalytic reduction process if the initial concentration of pollutant is low [30,31]. Where C_0 and C_t are the concentrations of the pollutants at time 0 and t, respectively, and k is the pseudo-first order rate constant. As can be observed, the photocatalytic reaction kinetics of 4-NA photocatalytic reduction can be fitted by the pseudo-first order model from linear curve fit based on the experimental data. It is easy to observe from Fig. 6(b) that the 4-CdS-M68 NCs exhibits the best photocatalytic degradation efficiency (0.5199 min^{-1}) among all the samples, which is about 32 and 4 times higher than that of MIL-68(Fe) (0.01603 min^{-1}) and CdS (0.1416 min^{-1}), respectively,

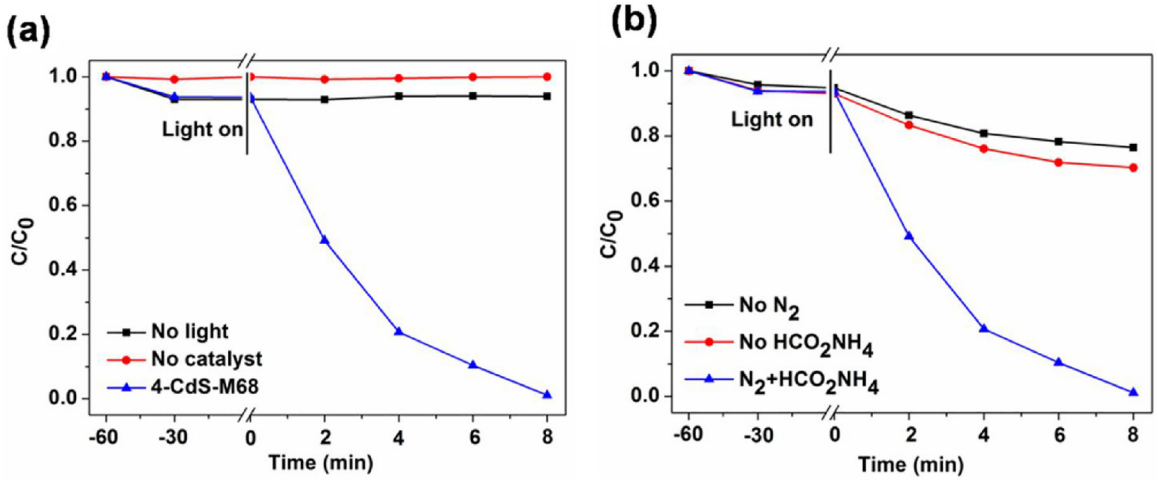

Fig. 5. (a) Control experiments of photocatalytic reduction of 4-NA under different conditions, (b) Comparison experiments of photocatalytic reduction of 4-NA under different conditions. Reaction conditions: 40 mg of photocatalyst, 40 mL of 20 ppm 4-NA, 20 mg of HCO_2NH_4, N_2 atmosphere.

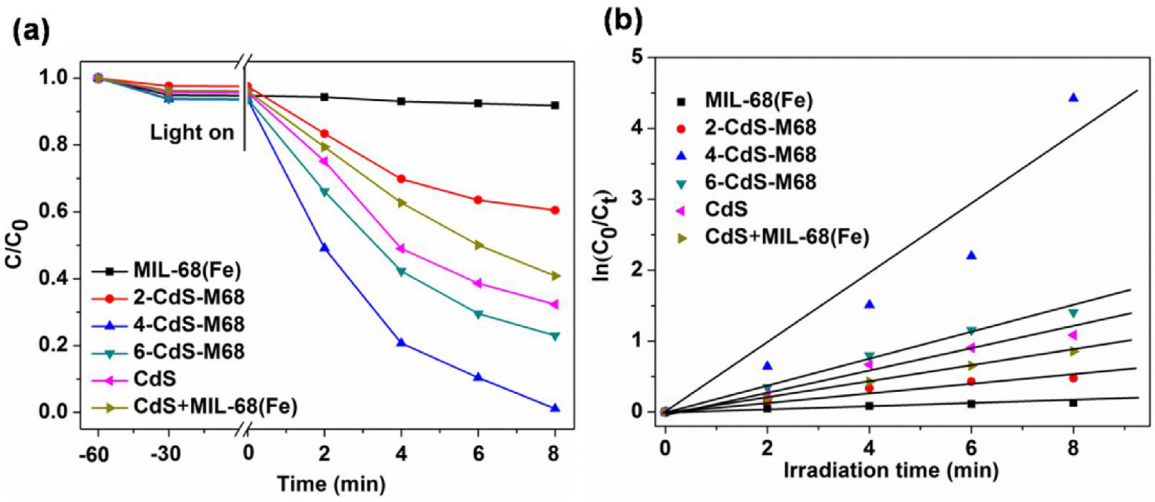

Fig. 6. (a) Photocatalytic selective reduction of 4-NA to 4-PDA over MIL-68(Fe), CdS, MIL-68(Fe) + CdS and the CdS-M68 NCs with different weight additions of CdS, (b) The pseudo-first order rate constants of 4-NA photocatalytic reduction over MIL-68(Fe), CdS, CdS-M68 NCs and MIL-68(Fe) + CdS. Reaction conditions: 40 mg of photocatalyst, 40 mL of 20 ppm 4-NA, 20 mg of HCO_2NH_4, N_2 atmosphere.

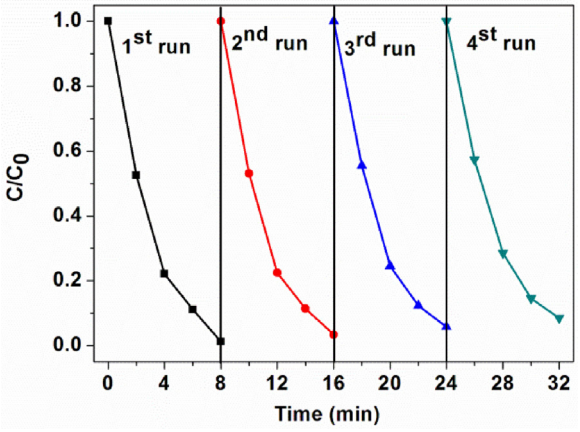

Fig. 7. Reusability of CdS-M68 NCs for photocatalytic reduction of 4-NA to 4-PDA. Reaction conditions: 40 mg of photocatalyst, 40 mL of 20 ppm 4-NA, 20 mg of HCO_2NH_4, N_2 atmosphere.

suggesting the high efficiency of 4-CdS-M68 NCs under visible light irradiation (see Table S1). To understand the influence of various supporters, a series of 4-CdS-supporter (supporter = TiO_2, C_3N_4, MIL-125(Ti) and MIL-125(Ti)-NH_2) have been fabricated *via* the photodeposition technique (incident light at $\lambda \geq 420$ nm for 4 h) and applied to photoreduction of 4-NA to PPD. Obviously, different kinds of supporters result in remarkably different photocatalytic activities of 4-CdS-supporter (see Fig. S4). Among all of the samples, the 4-CdS-M68 NCs exhibit the highest photocatalytic activity, giving a 4-NA conversion of ~100% after irradiation for 8 min.

3.3. Reusability and stability of CdS-M68 NCs

Generally, the stability of photocatalyst is a very important factor for its practical applications. After each cycling experiment, the photocatalyst was separated from the aqueous suspension by filtration, washed with ethanol several times to completely remove the absorbed 4-NA on the surface of sample. And then, the photocatalyst was centrifuged and dried under vacuum at 100 °C for 5 h. As shown in Fig. 7, the photostability of 4-CdS-M68 is verified by four successive recycling tests for reduction of 4-NA under visible light irradiation. Moreover, the XRD patterns, TEM images and XPS spectra (see Fig. S5, Fig. S6 and Fig. S7) of the fresh and used sample reveal the crystalline, morphology and surface chemical compositions of 4-CdS-M68 still keep unchanged even after the four cycles of the reaction. Additionally, the amount of Fe/Cd ions leaching during the reaction and the amount of CdS on MIL-68(Fe) after the reaction have been quantified by ICP optical emission spectrometer. Apparently, there is almost no Fe and Cd ions leaching from the 4-CdS-M68 during the reaction (see Table S2). It can be also found that the loading percentage of CdS in samples of 2-CdS-M68, 4-CdS-M68 and 6-CdS-M68 almost keep unchanged after the reaction, respectively (see Table S3). It should be noted that, for CdS-M68 NCs, the existence of MIL-68(Fe) can effectively restrain the reaction between the holes and CdS, resulting very few holes on CdS to cause photocorrosion. Moreover, in our reaction system, photogenerated holes are quenched by the addition of HCO_2NH_4, which is able to further prevent the photocorrosion of CdS during the photocatalytic reduction reaction [32]. The recycling tests indicate that the as prepared CdS-M68 photocatalysts have good anti-photocorrosion property.

3.4. Mechanism for the 4-NA photocatalytic reduction over CdS-M68 NCs

Electrochemical analysis of the MIL-68(Fe) has been carried out in our previous work [18]. The flat-band potential (V_{fb}) of the MIL-68(Fe) is around −0.60 V *vs.*NHE, which is more negative than the redox potential of Cd^{2+}/Cd^0 ($E_{(Cd2+/Cd0)}$ = −0.41 V *vs.* NHE) [20]. On the other hand, the V_{fb} of the as-prepared CdS is around −1.1 V *vs.* NHE, and the calculated conduction band potential (V_{CB}) is equal to 1.24 V *vs.* NHE (see Fig. S8). The matched band potentials between MIL-68(Fe) and CdS make it theoretically feasible for CdS to transfer the photogenerated electrons in its CB to MIL-68(Fe) under visible light irradiation, thus, effective transportation of the photogenerated electrons and holes could be achieved. Electrochemical analyses have been used to further investigate the effective transportation of the photongenerated carrieies over CdS-M68 NCs. Fig. 8 shows the transient photocurrent-time (I-t) curves of CdS-M68 NCs under intermittent visible light illumination with the wavelength range used in the photocatalytic reactions. It is obvious that light irradiation of the CdS-M68 film coated on FTO glass shows a strong photocurrent response and the photocurrent rapidly decreases to zero as long as the light is switched off. Thus, the result indicates that these photogenerated carriers can be efficiently separated upon contact with a high work function conductor.

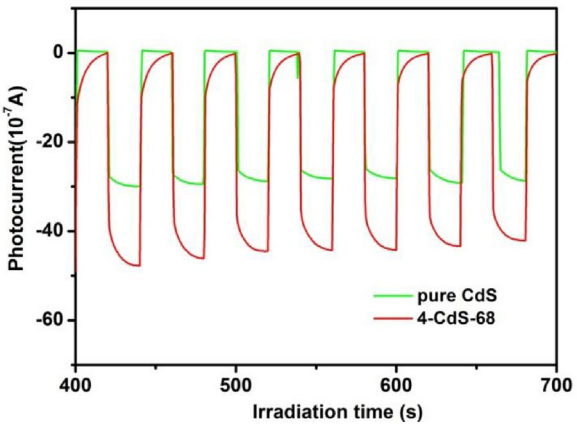

Fig. 8. Transient photocurrent response of pure CdS and 4-CdS-M68 in 0.2 M Na_2SO_4 aqueous solution under irradiation of visible light ($\lambda \geq 420$ nm).

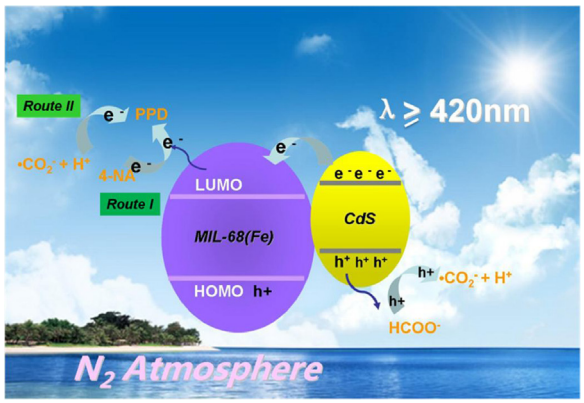

Fig. 10. Possible mechanism of photocatalytic selective reduction of 4-NA to 4-PDA over CdS-M68 NCs.

To further investigate the major active species during reduction of nitro organics, the trapping experiments have been performed, using $K_2S_2O_8$ as scavenger for photogenerated electrons. As displayed in Fig. 9(a), about 25.4% suppression are observed when $K_2S_2O_8$ is added into 4-NA in the aqueous phase over 4-CdS-M68 NCs. It is manifesting that although photogenerated electrons are involved in the 4-NA photocatalytic reduction, there may existing some other active species in this photocatalytic process. This inference could be further verified by the 5,5-dimethyl-1-pyrroline *N*-oxide (DMPO) spin-trapping electron spin resonance (ESR) technique. Fig. 9(b) shows that sextet characteristic peaks of the DMPO-$^{\bullet}CO^{2-}$ adduct are clearly observed in the presence of HCO_2NH_4 under visible light irradiation. The formation of the $^{\bullet}CO^{2-}$ radicals can be attributed to the reaction between the photoexcited holes of the photocatalyst and HCO_2NH_4 ($E_{HCO2/CO2} = 1.07$ V *vs.* NHE) [33]. Photoinduced electrons and $^{\bullet}CO^{2-}$ radicals have strong reductive powers ($E_{CB}(CdS) = -1.1$ V *vs.* NHE; $E_{(^{\bullet}CO2-/CO2)} = -2.2$ V *vs.* NHE, pH = 6.8). Therefore, these species can efficiently reduce 4-NA to PPD ($E_{(4\text{-}NA/PPD)} = -0.67$ V *vs.* NHE) in water under N_2 atmosphere [4,5]. The result reveals that HCO_2NH_4 not only serves as a hole scavenger to suppress the photocorrosion of the CdS-M68 NCs, but also can produce an active species ($^{\bullet}CO^{2-}$ radicals) in the present system.

Accordingly, a probable mechanism has been proposed, as illustrated in Fig. 10. Under visible-light irradiation ($\lambda \geq 420$ nm), the CdS and MIL-68(Fe) are both photoexcited to generate charge carriers. The photogenerated electrons of CdS can transfer to MIL-68(Fe) owing to their intimate interfacial contact and matchable energy band position. The electrons could reduce the adsorbed 4-NA. It is reasonable because the overall photoreduction of aromatic nitro organics to corresponding amino organics can be expressed by the Route I (in Fig. 10). Simultaneously, the HCO_2NH_4 serves as an efficient scavenger that could capture the holes to form $^{\bullet}CO_2^-$ radicals. The $^{\bullet}CO_2^-$ radicals possess a strong reduction capacity and can also efficiently reduce 4-NA to PPD (Route II in Fig. 10). In addition, the N_2 purge provides an anaerobic atmosphere for the reaction. Thus, the aromatic nitro organics have no opportunity to undergo the oxidation reaction. Meanwhile, the presence of MIL-68(Fe) also increases the accumulating concentration of 4-NA over the surface of CdS-M68 NCs. As a result, the adsorbed 4-NA can be effectively reduced to PPD by accepting photogenerated electrons and $^{\bullet}CO_2^-$ radicals from CdS-M68 NCs under visible light irradiation.

4. Conclusions

In summary, we prepared a series of CdS-M68 NCs with different irradiation times via a facile approach by simply photodepositing CdS on the surface of MIL-68(Fe). The amount of generated CdS and the optical band gap of the nanocomposites were widely tunable by changing the irradiation time. Results demonstrated that the as-prepared 4-CdS-M68 NCs shown excellent photocatalytic activity for the photoreduction of 4-NA to PPD in water under visible light ($\lambda \geq 420$ nm), giving a 4-NA conversion of ~100% and high PPD selectivity after irradiation for 8 min. The significantly enhanced photoactivity could be attributed to the synergistic effect of the

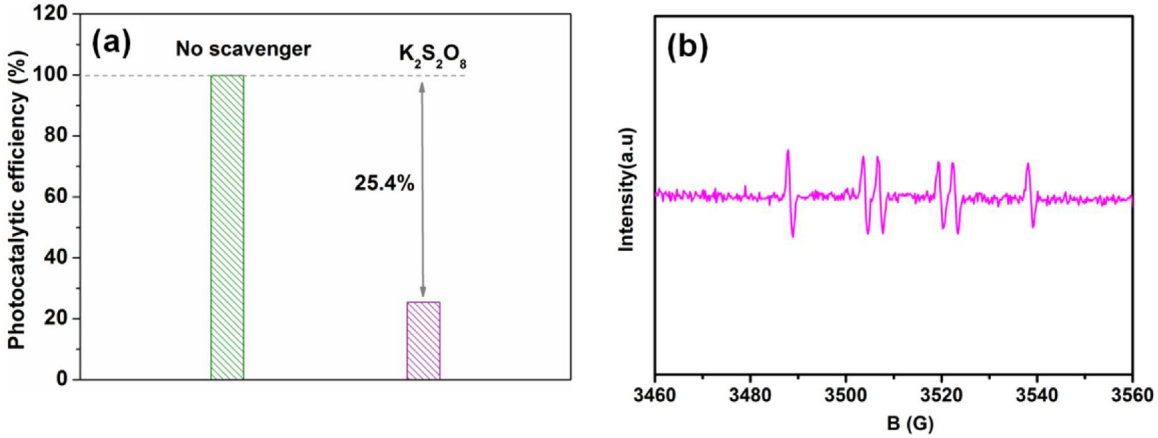

Fig. 9. (a) The photocatalytic reduction of 4-NA over CdS-M68 under visible light irradiation in the presence of $K_2S_2O_8$, (b) DMPO spin-trapping ESR spectrum of 4-CdS-68 in water dispersion.

effective transportation of the photogenerated electron-hole pairs and the enhanced visible light absorption intensity. Further results revealed that the photoexcited electrons and $\bullet CO_2^-$ radicals as the main active species process strong reduction capacity to reduce the surface adsorbed 4-NA. This work not only offers new insight into the design and fabrication of MOF-semiconductor photocatalysts, but also providing a simple and highly efficient route for the preparation of aminobenzenes by using MOF-based photocatalysts under visible light irradiation in water.

Acknowledgements

This work was supported by the National Natural Science Foundation of China (51672048 and 21473096) and the Major Science and Technology Projects of Fujian Province (2015YZ0001-1).

Appendix A. Supplementary data

Supplementary data associated with this article can be found, in the online version, at http://dx.doi.org/10.1016/j.apcatb.2017.06.075.

References

[1] Z. Dong, X. Le, X. Li, W. Zhang, C. Dong, J. Ma, Appl. Catal. B: Environ. 158–159 (2014) 129–135.
[2] I. Ibrahim, I.O. Ali, T.M. Salama, A.A. Bahgat, M.M. Mohamed, Appl. Catal. B: Environ. 181 (2016) 389–402.
[3] B. Weng, S. Liu, N. Zhang, Z.R. Tang, Y.J. Xu, J. Catal. 309 (2014) 146–155.
[4] W. Wu, L. Wen, L. Shen, R. Liang, R. Yuan, L. Wu, Appl. Catal. B: Environ. 130–131 (2013) 163–167.
[5] W. Wu, R. Lin, L. Shen, R. Liang, R. Yuan, L. Wu, Phys. Chem. Chem. Phys. 15 (2013) 19422–19426.
[6] A.J. Wang, H.Y. Cheng, B. Liang, N.Q. Ren, D. Cui, N. Lin, B.H. Kim, K. Rabaey, Environ. Sci. Technol. 45 (2011) 10186–10193.
[7] D. Meissner, R. Memming, B. Kastening, J. Phys. Chem. 92 (1988) 3476–3483.
[8] C. Venkata Reddy, R. Ravikumar, G. Srinivas, J. Shim, M. Cho, Mater. Sci. Eng. B 221 (2017) 63–72.
[9] N. Qin, J. Xiong, R. Liang, Y. Liu, S. Zhang, Y. Li, Z. Li, L. Wu, Appl. Catal. B: Environ. 202 (2017) 374–380.
[10] S.W. Cao, Y.P. Yuan, J. Fang, M.M. Shahjamali, F.Y.C. Boey, J. Barber, S.C. Joachim Loo, C. Xue, Int. J. Hydrogen Energy 38 (2013) 1258–1266.
[11] X. Dai, M. Xie, S. Meng, X. Fu, S. Chen, Appl. Catal. B: Environ. 158–159 (2014) 382–390.
[12] G. Férey, Chem. Soc. Rev. 37 (2008) 191–214.
[13] F.X. Llabrés i Xamena, A. Corma, H. García, J. Phys. Chem. C 111 (2006) 80–85.
[14] R. Liang, F. Jing, L. Shen, N. Qin, L. Wu, J. Hazard. Mater. 287 (2015) 364–372.
[15] R. Liang, L. Shen, F. Jing, W. Wu, N. Qin, R. Lin, L. Wu, Appl. Catal. B: Environ. 162 (2015) 245–251.
[16] M. Wen, K. Mori, Y. Kuwahara, H. Yamashita, ACS Energy Lett. 2 (2017) 1–7.
[17] M. Wen, Y. Cui, Y. Kuwahara, K. Mori, H. Yamashita, ACS Appl. Mater. Interfaces 8 (2016) 21278–21284.
[18] F. Jing, R. Liang, J. Xiong, R. Chen, S. Zhang, Y. Li, L. Wu, Appl. Catal. B: Environ. 206 (2017) 9–15.
[19] F. Ke, L. Wang, J. Zhu, Nano Res. 8 (2015) 1834–1846.
[20] L. Shen, S. Liang, W. Wu, R. Liang, L. Wu, J. Mater. Chem. A 1 (2013) 11473–11482.
[21] W. Zhan, Q. Kuang, J. Zhou, X. Kong, Z. Xie, L. Zheng, J. Am. Chem. Soc. 135 (2013) 1926–1933.
[22] J. Hong, C. Chen, F.E. Bedoya, G.H. Kelsall, D. O'Hare, C. Petit, Catal. Sci. Technol. 6 (2016) 5042–5051.
[23] X. Zeng, L. Huang, C. Wang, J. Wang, J. Li, X. Luo, ACS Appl. Mater. Interfaces 8 (2016) 20274–20282.
[24] A. Fateeva, P. Horcajada, T. Devic, C. Serre, J. Marrot, J.M. Grenèche, M. Morcrette, J.M. Tarascon, G. Maurin, G. Férey, Eur. J. Inorg. Chem. 2010 (2010) 3789–3794.
[25] C. Yu, L. Gou, X. Zhou, N. Bao, H. Gu, Electrochim. Acta 56 (2011) 9056–9063.
[26] S. Bordiga, C. Lamberti, G. Ricchiardi, L. Regli, F. Bonino, A. Damin, K.P. Lillerud, M. Bjorgen, A. Zecchina, Chem. Commun. (2004) 2300–2301.
[27] G.T. Vuong, M.H. Pham, T.O. Do, Dalton Trans. 42 (2013) 550–557.
[28] G.T. Vuong, M.H. Pham, T.O. Do, CrystEngComm 15 (2013) 9694–9703.
[29] X. Wu, J. Zhao, L. Wang, M. Han, M. Zhang, H. Wang, H. Huang, Y. Liu, Z. Kang, Appl. Catal. B: Environ. 206 (2017) 501–509.
[30] I.K. Konstantinou, T.A. Albanis, Appl. Catal. B: Environ. 49 (2004) 1–14.
[31] S. Chakrabarti, B.K. Dutta, J. Hazard. Mater. 112 (2004) 269–278.
[32] W. Wu, G. Liu, Q. Xie, S. Liang, H. Zheng, R. Yuan, W. Su, L. Wu, Green Chem. 14 (2012) 1705–1709.
[33] J. Belloni, M. Treguer, H. Remita, R. De Keyzer, Nature 402 (1999) 865–867.